Journal of Materials Chemistry A

PAPER

View Article Online
View Journal | View Issue

Cite this: J. Mater. Chem. A, 2018, 6, 17481

Three dimensional modelling of the components in supercapacitors for proper understanding of the contribution of each parameter to the final electrochemical performance†

Farshad Barzegar, ‡*[a] Lijun Zhang,‡[a] Abdulhakeem Bello,[bc] Ncholu Manyala [b] and Xiaohua Xia[a]

Received 21st May 2018
Accepted 16th August 2018

DOI: 10.1039/c8ta04736g

rsc.li/materials-a

Three dimensional (3D) modelling of supercapacitors (SCs) has been investigated for the first time to have a better understanding of and study the effect of each parameter on the final electrochemical results. Based on this model, the resistance of the electrolyte, membrane, current collectors and active materials have effects on the first intersection points on the real axis (*x*-axis) of the Nyquist plots (equivalent series resistance (ESR)). These results indicate inward shrinking of the cyclic voltammograms (CV) due to a small change in the leakage resistance and resistance of the faradic component of materials, and they also explain the parameters that lead to the deformation of the CV from ideal behaviour. The 3D model was verified with experiments using activated carbon-based SC devices. The experimental results confirmed the 3D model results and suggested that the proposed 3D model is reliable and can be used for the proper design of SC devices.

Introduction

Storage systems with sufficient capacity and highly efficient charge and discharge characteristics are of huge and strategic importance for portable electronics and biomedical applications, as well as for short and medium-term stationary applications. For these purposes, different technologies are being developed including mechanical, thermal, physical, chemical and electrochemical energy storage systems.[1] An advanced solution is to use batteries with high energy densities, however, they suffer from low power densities, short cycle lives, safety risks and poor adaptability with flexible systems.[2] Electrochemical capacitors (ECs), also called supercapacitors, with high power densities, good cycling stabilities, and fast charge–discharge rates are new energy storage devices that have attracted attention in the scientific community.[3–5] Currently, research in the field of supercapacitors is focused on fine-tuning electrodes, electrolytes and material sections to achieve the best performance.[6–8] However, there are no studies on the effect of the resistances of each parameter on the final electrochemical performance, which could help researchers to develop and synthesize the best ECs depending on the usage.

For a better understanding of ECs, we need to understand the full behavior of each component of the EC during charge and discharge. Based on their charge storage mechanism, ECs can be classified as electric double layer capacitors (EDLCs), pseudo-capacitors or redox electrochemical capacitors (RECs) and hybrid electrochemical capacitors.[9] The EDLCs store energy by a charge separation at the electrode–electrolyte interface,[10] while REC materials not only store energy like EDLCs, but also in the appropriate potential window undergo electrochemical faradaic reactions between the electrode materials and ions.[11] Until now most researchers have tried to explain the electrical behavior of pure EDLCs[12] for ECs, however, none of the reports clearly explain the effects of the resistances of each component of ECs and how this reflects in their behavior that leads to the final stored energy. In this article, we study and provide a deep understanding of the electrical behavior of ECs and the effect of each component on the final electrochemical performance. Verification and confirmation of the proposed model was carried out experimentally with activated carbon-based materials and a KOH aqueous electrolyte in the laboratory.

Modelling of the supercapacitor

The electrical behavior of ECs can be described by the lumped-element impedance-based model. The most common models

[a]Electrical, Electronic and Computer Engineering Department, University of Pretoria, Pretoria 0002, South Africa. E-mail: farshadbarzegar@gmail.com

[b]Physics Department, Institute of Applied Materials, SARCHI Chair in Carbon Technology and Materials, University of Pretoria, Pretoria 0028, South Africa

[c]Department of Materials Science and Engineering, African University of Science and Technology, Abuja, Nigeria

† Electronic supplementary information (ESI) available. See DOI: 10.1039/c8ta04736g

‡ The first two authors contributed equally to this work.

for the description of EDLCs are in three categories, namely a RC circuit model, a three branch RC circuit model, and a transmission line model (Fig. 1). The simple RC circuit model, as shown in Fig. 1(a), includes four ideal circuit elements: the R_S element represents series resistance which is due to the presence of an electrolyte and metallic conductors, the L element represents the series inductance that is mostly influenced by the geometry of the connectors and electrodes, C is the ideal behavior of a capacitor which stores energy by charge separation at the electrode–electrolyte interface and the R_{CT} element is present due to the process of charge transfer from the electrode to the electrolyte and leakage current. The loss in energy of EDLCs, during self-discharge, charging and discharging, gives rise to leakage of current resistance caused by equivalent series resistance (ESR).[13,14] It is necessary to extend the simple RC circuit model since it cannot be used to probe the porous nature of electrodes or show the behavior of EDLCs accurately over a frequency range.

The three branch RC circuit presented by L. Zubieta and R. Bonert[15] is shown in Fig. 1(b). It consists of the leakage resistance R_{LK} in parallel to three branches which correspond to different time constants for charge transfer. The first or immediate branch is for the time range of seconds and it consists of a resistance R_i in series with two capacitors: a voltage dependent capacitor C_{i1} and a normal capacitor C_{i0}. The delayed branch, with parameters R_d and C_d, represents time constants within the minutes range while the long term branch, containing R_l and C_l, represents time constants greater than ten minutes. The model shows a suitable connection with experimental results, however, the model has a weakness in that the circuit components lack physical meaning.[16]

The transmission line model is adopted in many reports[17,18] to precisely represent the porous nature of the electrodes in EDLCs as shown in Fig. 1(c). This model includes leakage resistance R_{LK}, solution resistance R_{el}, electrode resistance R_{ed}, inductance L_S which prevails at high frequency, and a resistance R_P that is in parallel with inductance L_P which are observed above resonant frequency.

All of the above mentioned models are incomplete models for actual ECs and cannot be used to examine the resistances of each parameter of ECs (the active material, the electrolyte, the separator *etc.*) individually and their focus is mostly on the EDLC material. Thus, in this paper, we propose a realistic three dimensional model to study and elucidate the resistances of each component of ECs individually and the influence of each component on the final behavior of ECs. Cyclic voltammetry (CV) and galvanostatic charge–discharge (GCD) modeling and measurements cannot be completely understood in the electrochemical reaction at the electrode–electrolyte interface but a complete description can be explained using electrochemical impedance spectroscopy (EIS).[19] EIS is often represented by a Nyquist plot which presents the real (x-axis) and imaginary parts of the impedance (y-axis). The Nyquist plot takes into account the different parameters (resistance, capacitance, inductance *etc.*) that are all dependent on the frequency and it is usually divided into three regions of low frequency, medium frequency and high-frequency.[20] For an ideal capacitor, the Nyquist plot of impedance is represented by a vertical line which is parallel to the imaginary axis (y axis), which is only correct for liquid mercury electrodes. The impedance of most solid electrodes deviates from purely capacitive behavior.[21]

To offer a realistic model close to the practical situation, the behavior of ECs should be described by a complex network of non-linear inductances, capacitances and resistances. Thus, Fig. S1(a) and (b)† have been proposed for realistic and accurate 2D modelling of the ideal behavior of EDLC and REC material respectively. The ECs shown in Fig. 2 and S1,† depend on several parameters, such as the capacitors that present double layer behavior (C_1 and C_2), the capacitors that present redox electrochemical behavior (C_{F1} and C_{F2}), inductance (L), resistance of the electrolyte (R_e), a current collector and the resistance of the electrode material (R_C), the membrane resistance (R_m), the faradic part of the material resistance (R_f) and the leakage resistance (R_{lk}) (that is dependent on packaging). The suggested RECs model in our simulation is based on behavior that is close to battery materials,[22,23] due to the fact that most oxide materials for RECs show a faradaic phenomenon. In reality, the presence of functional groups at the surface of the electrode materials for EDLCs cannot be overruled, and these

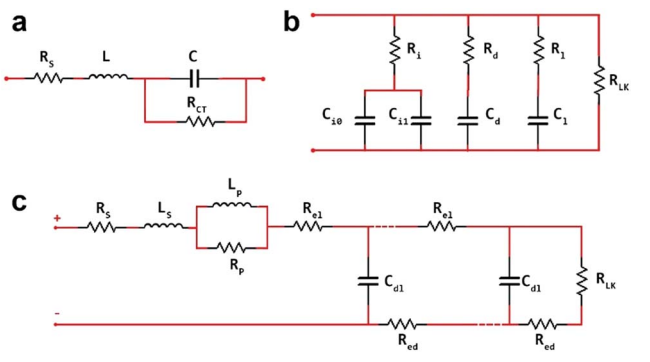

Fig. 1 EDLC: (a) a simple RC circuit model, (b) a three RC circuit model and (c) a transmission line model.

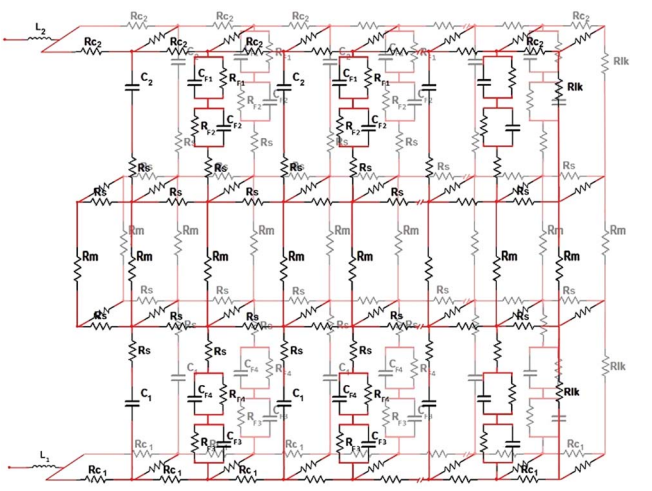

Fig. 2 3D electrical equivalent model of practical ECs.

materials show similar behavior to RECs during charge and discharge, contributing a pseudo-capacitive effect to the total electrochemical performance. Similarly, some oxide materials such as RuO and MnO_2 exhibit (pseudo) EDLC behavior [24] and this makes their models complex. To resolve these issues, the final 2D model presented in Fig. S1(c)† considers a hybrid model that takes care of all the functional groups and other parameters, bringing the model close to the practical EC behavior. Lastly, a 3D hybrid model in Fig. 2 (Fig. S1(d)†) was suggested for a realistic simulation of the behavior of EDLCs.

Methods

Simulation of the full cell supercapacitor

In order to study the performance of the passive hybrid system and to verify the analytical approach above, simulations in Matlab/Simulink were conducted using Simpower GUI. A sawtooth wave with the maximum voltage of 1 V and frequency of 0.01 was used to charge and discharge the cell in order to simulate its performance. Firstly, the 2D model was built in Simulink as shown in Fig. S2.† The two 2D models in Fig. S2† were then connected together through two resistor banks, each comprising R_e and R_C, to form the 3D model shown on the right hand side of Fig. S3.† The left hand side of Fig. S3† shows the charge/discharge control and output voltage and current measurement circuit, where Isc.mat and Vsc.mat store the simulated current and voltage profiles of the cell and Vchg.mat provides the sawtooth voltage waveform of the charge/discharge data given in Fig. S4.†

Experimental and electrode preparation of the full cell supercapacitor

Polymer based activated carbon (AC) was used in the experimental section and was prepared by the methods reported in our previous work[25] using hydrocarbons such as polyvinyl alcohol (PVA)/polyvinylpyrrolidone (PVP) as a source of carbon, through chemical activation with KOH as the active agent to produce the desired porous carbons. The porous carbon (activated carbon (AC)) that was used for the electrochemical tests had a surface area of 1063 $m^2\ g^{-1}$ and had some functional groups on the surface as explained in our previous work. The electrodes were made by combining the active materials, the conductive additive (carbon black) and polyvinylidene fluoride (PVDF) in *N*-methyl pyrrolidone (NMP) to make a slurry which was coated on a nickel foam that was graphene coated as a current collector and dried at 60 °C in an oven overnight. The device was tested in a two-electrode configuration with a microfiber filter paper (thickness of 180 μm with 11 μm pore size (particle retention)) as a separator. Three set of devices were made and tested numerous times to ascertain the reproducibility before coming to a conclusion. The reference cell and the first device consisted of the active material (activated carbon with functional groups) derived from PVA\PVP, carbon black and PVDF with weight ratios of 90%, 5% and 5% respectively, 6 M KOH, one glass microfiber filter paper separator and a graphene coated nickel foam current collector. Furthermore, the resistance of the active material (R_C) in the second device was increased by increasing the binder by 10% without the addition of a conductive agent (carbon black). The third device was made with the intention of increasing the resistance of the electrolyte (R_e), where 5 ml of a 10 wt% PVA solution was added to 5 ml of 6 M KOH. The number of the separators was also increased so as to slow the movement of ions within the electrodes which will result in increased membrane resistance (R_m). It is worth stating that it is quite difficult to control all other parameters in reality and thus all the test parameters were repeated numerous times to confirm the results obtained. Electrochemical measurements (electrochemical impedance spectroscopy (EIS) and cyclic voltammetry (CV)) were carried out using a Bio-logic VMP-300 potentiostat. The EIS measurements were conducted in the frequency range from 0.01 Hz to 100 kHz with the open circuit potential of ~0 V.

Results and discussion

To study the effects of the resistances of each parameter separately and how they reflect in the final electrochemical performance, a reference cell was necessary. After the 3D model of the supercapacitor was designed, each parameter of the cell was assigned a specific value and the outcome of that was considered as the reference cell result. Then, to study the parameter effects individually, each parameter was changed separately while the rest of the parameters were fixed at reference values. To see the negative effect of each parameter compared to the reference cell, some of the parameters were increased and some were decreased. The modified value was just a number that was high enough to see the effect of each parameter compared to the reference cell. Fig. 3 displays the EIS plot, the phase angle *versus* frequency and the CV curves of the simulation results after changing the resistance of each parameter compared to the reference cell. In our simulation results, R_e represents the resistance of the electrolyte, R_m is the resistance of the membrane, R_C is the resistance of the current collector and the electrode materials, R_{lk} is the leakage resistance and R_{CT} is the resistance of the faradic part of the material. It is clear that each parameter had a different effect on the final result of the supercapacitor. For better understanding and clarity of the results, each parameter was plotted and investigated separately compared to the reference cell.

Fig. 4(a) and (b) present the effects of the electrolyte resistance on the final results of the EIS plot and CV curves. As observed from Fig. 4(a) a change in the resistance of the electrolyte (R_e) by a factor of 100 led to an increase in the first intersection points on the real axis (*x*-axis) of the Nyquist plots. This frequency plot corresponds to the typical time constants in most high-power applications, and for intermediate frequencies, the complex-plane plots form an angle of ~45° with the real axis as seen in the figure. This angle is explained by the limited current penetration into the porous structures of the electrodes.[26] For lower frequencies, the spectra approach a nearly vertical line in the complex plane, which is typical of ideal capacitors. Similarly, a shift and increase in the high-frequency area and the angle of the Nyquist plots for the

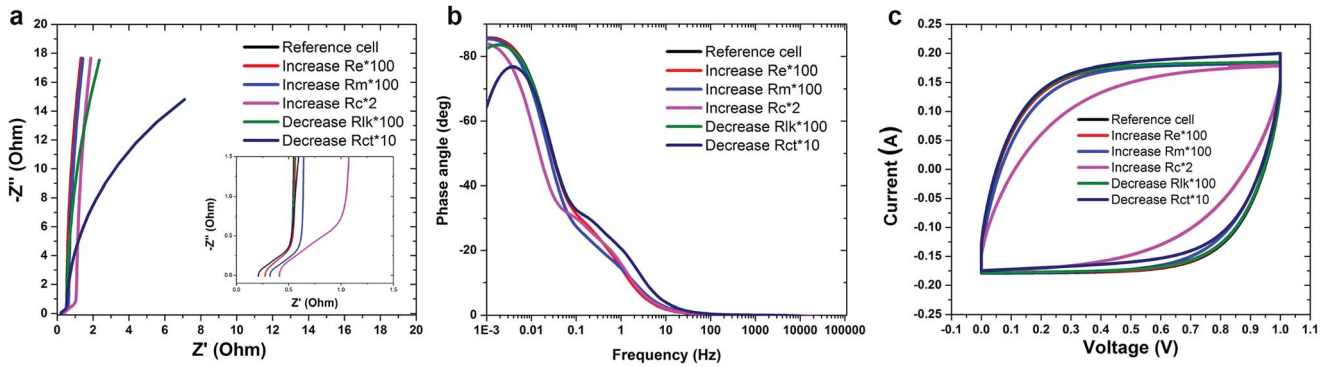

Fig. 3 (a) EIS plot, (b) the phase angle *versus* frequency and (c) CV curves of the simulation results.

intersection of the high and medium-frequency regions was also observed. The model has a highly dynamic load at the beginning as well as deeper charging and discharging. The corresponding CV and the calculated data show excellent agreement. Fig. 4(b) shows the CV curves of the simulated results based on the reference cell and the simulated cell after the R_e was increased by 100 times indicating that there was no change in the shape of the CV, and rather a small decrease in current was observed which corresponded to a slight shrinkage of the CV. This also indicates a decrease in the capacitance of the device.

Several other components contribute to the overall performance of the device, such as the membranes that prevent short-circuiting within the device. Fig. 4(c) and (d) present the effect of the membrane (separator) resistance on the final performance of the device. Fig. 4(c) shows an increase in the resistance of the membrane (R_m) by a factor of 100 and shows that the first intersection points on the real axis (x-axis) of the Nyquist plots increased and the whole plots shifted by the same length. The angle of the Nyquist plots for the intersection of the high and medium-frequency regions did not change. The corresponding CV in Fig. 4(d) shows a similar result with a shrunken CV indicating a capacitive decrease. It is clear that the results obtained using the proposed model give similar results to what was obtainable in the experiments that are presented at the end of the paper. Therefore, the proposed electric model can be used in designing a voltage controller and in sizing a supercapacitor for storage applications.

The resistances of the current collectors and active materials (and resistance at the interface of them) also play a crucial part in the performances of the devices. Such contributions are presented in Fig. 5. Fig. 5(a) and (b) show the results of increasing the resistance of the current collector and the electrode materials (R_C) by a factor of 2 (the parameter that was chosen for R_C for the reference cell was high at first, so an increase by a factor of 2 made it high enough to see the effect of R_C compared to the reference cell). From Fig. 5(b) which provides an enlarged view of the Nyquist plot, the remarkable deviations shown were attributed to the longer time taken for charge to reach the surface of the active material. These deviations could also affect the efficiency of the device which is influenced by the resistance of the electrodes which means that increasing the real part of the impedance with a corresponding decrease in frequency has to be taken into consideration. However, the angle of the Nyquist plots for the intersection of the high and medium-frequency regions remained the same. Fig. 5(c) shows a clear shrinkage in the CV that explains a decrease in the performance of the device, hinting that the resistance of the active material and the current collector play a crucial part in the performance of the electrochemical devices. The shrinking might be attributed to a number of factors such as, the conductivity, and the pore dimensions of the active materials and the current collectors.

Fig. 6 presents the effect of leakage resistance (R_{lk}) on the final results. Fig. 6(a) and (b) show that by decreasing the R_{lk} by 100 times, the first intersection points on the real axis (x-axis) of

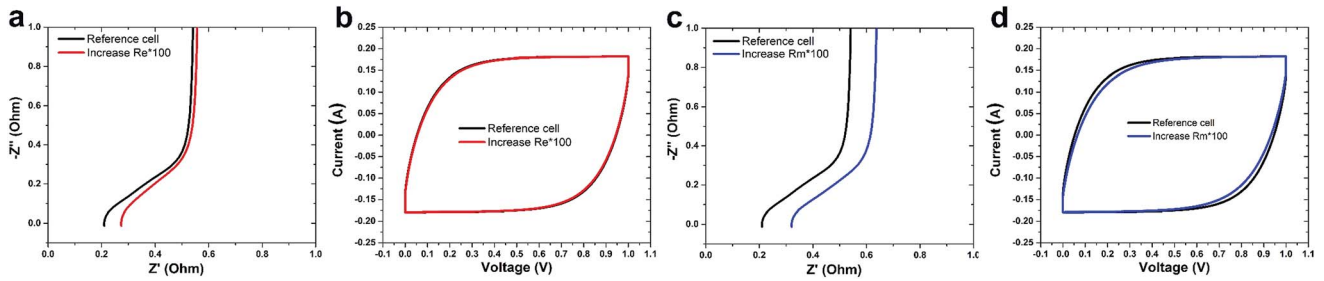

Fig. 4 Simulation results of the EIS plot and CV curves (a) and (b) when increasing the resistance of the electrolyte 100 times, and (c) and (d) when increasing the membrane resistance 100 times.

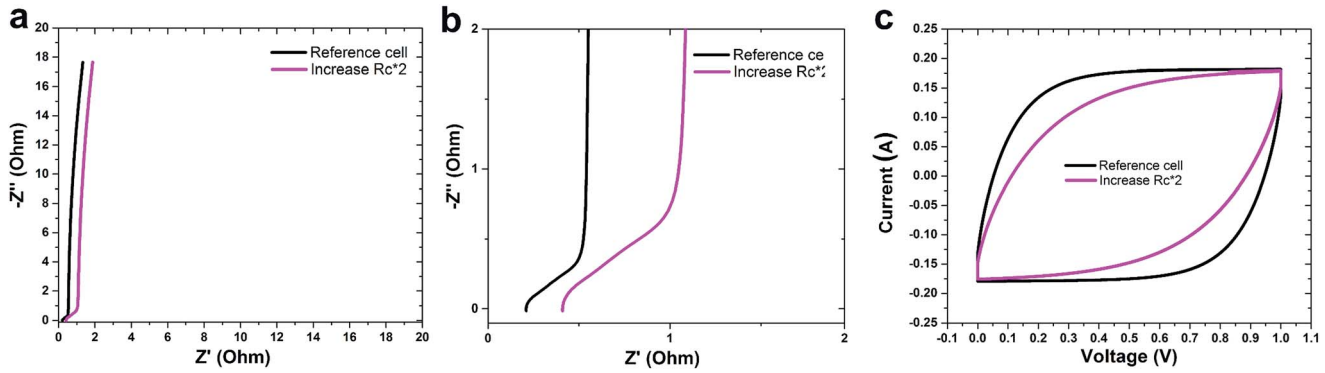

Fig. 5 Simulation result (a) and (b) of the EIS plots and (c) the CV curves when increasing the resistance of the current collectors and active materials 2 fold.

the Nyquist plots did not change. Decreasing the R_{lk} had a negative effect on the capacitance of the supercapacitor. The only part affected was the low-frequency region that shows more deviation from the vertical lines. Decreasing the R_{lk} meant that the cell had an easier way to discharge than keeping the charge at the surface. Fig. 6(c) and (d) show CV curves of the simulation results of the reference cell and the cell after decreasing R_{lk} by 100 times. For the first time, this paper reports an upward shift and a shape change (pushed inward) of the CV curve by adjusting one parameter such as the leakage resistance (Fig. 6) or the resistance of the faradic part of the materials (effect of functional groups) (Fig. 7). The initial and final points moved up and the shape of the CV curve was pushed inward a little. The shift in CV was more at the endpoint with the high current than the first point with the low current which was considered as a shift to match the initial point. As the EIS results showed, decreasing the R_{lk} had a negative effect on the capacitance of the supercapacitor, thus, by decreasing the R_{lk}, the supercapacitor needs more energy to charge than the energy given in the discharge section.

Fig. 7 presents the effect of the resistance of the faradic part of the material (R_{CT}) on the final results. As shown in Fig. 7(a) and (b), a decrease in the R_{CT} by 10 times led to no change in the intercept value on the real axis (x-axis) of the Nyquist plots, however, it introduced a negative effect on the faradic part of the performance of the supercapacitor. The only part that was affected was the low-frequency region that became more resistive and deviated from the vertical lines. Fig. 7(c) shows CV curves of the simulation results of the reference cell and the cell after decreasing R_{CT} by 10 times and it shows the same trend as Fig. 6(c) and (d). The initial and final points moved up and the shape of the CV curves was pushed inward a little. A decrease in the R_{CT} reduced the potential capacity of the capacitor that presented redox electrochemical behavior (C_F) and had a negative effect on the capacitance of the supercapacitor so that the EC needed more energy to charge than the energy given in the discharge section. The R_{CT} and C_F had a very close relationship to each other that was linked to the properties of the material.

Fig. 8 presents an enlarged view of the phase angle *versus* frequency of the simulations. This figure shows the effect of each parameter discussed above on the final result of the phase angle. The ideal capacitor phase angle should be $-90°$. The closer the phase angle is to $-90°$, the more similarly the device performs to an ideal capacitor.[27] Fig. 8 shows that all the EIS simulations showed a similar trend. Those parameters that provide more resistive behavior that influences the final capacity, move the phase angle far away from $-90°$.

For the purpose of verifying the analysis above and confirming the proposed model, experiments with an activated carbon-based supercapacitor were tested in the laboratory. In the experimental section, the parameters that it was possible to control physically in our laboratory were investigated. An investigation of the high-frequency region and effect of each resistive component of the device was carried out experimentally to ascertain and confirm the proposed three-dimensional hybrid model. We detected the same trend in Fig. 9 as the 3D

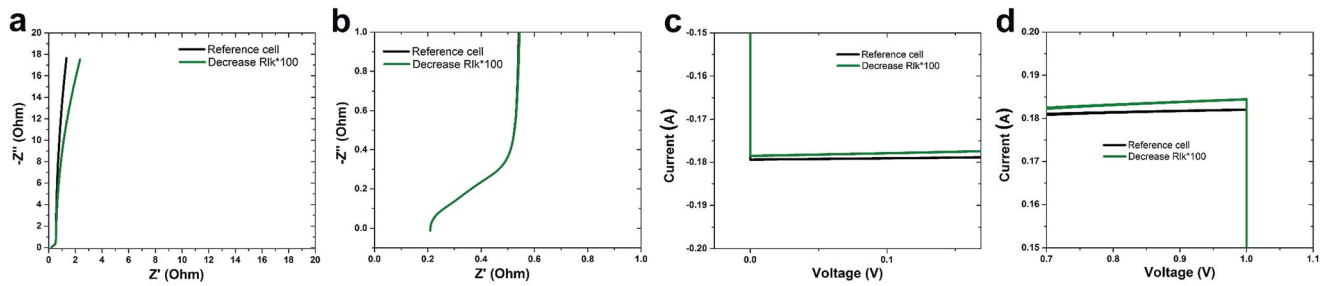

Fig. 6 Simulation results of the EIS plots (a) and (b) and CV curves (c) and (d) when decreasing the leakage resistance 100 fold.

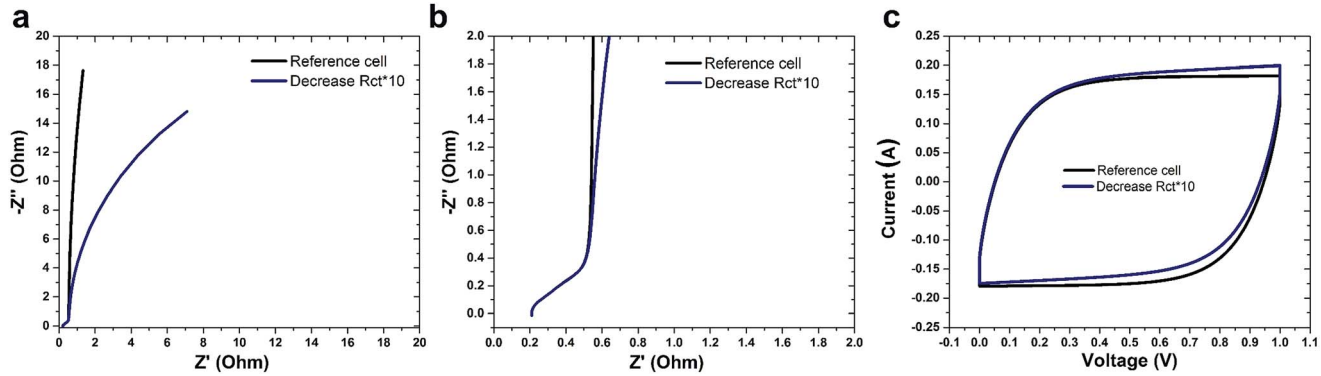

Fig. 7 Simulation result of the EIS plots (a) and (b) and CV curves (c) when decreasing resistance of the faradic part of the material 10 fold.

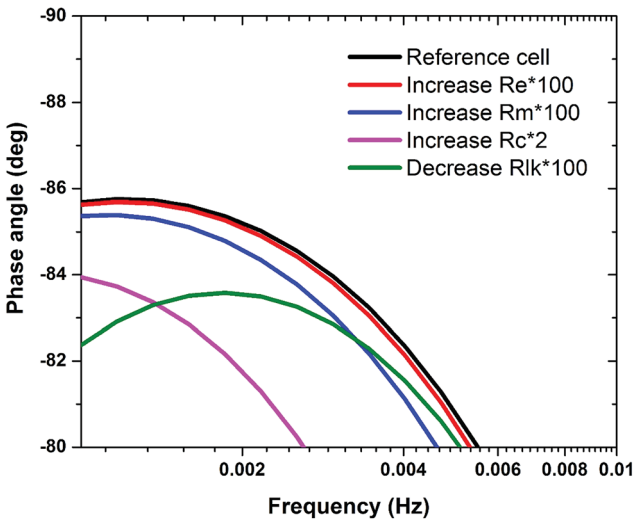

Fig. 8 An enlarged view of the phase angle *versus* frequency of the simulations.

simulation results proposed. However, as shown in Fig. 9(a), the length of the EIS increased after changing one parameter due to the fact that the mass of the material was not as completely uniform as that of the reference cell and the other cell. Controlling the mass at such a scale was very difficult with our equipment. The phase angles (Fig. 9(b) and S5†) and CV curves (Fig. 9(c)) of the experiments also followed the 3D model results that suggest that the proposed model was completely correct. By disregarding the mass effect on the capacity, the CV shape after increasing the R_e was almost the same as that of the reference cell. By increasing the R_m and R_C, clear shrinkage occurred in the CV shape as the 3D model also suggested.

Conclusion

In conclusion, a novel 3D model of a supercapacitor was presented. The results report the effect of each parameter individually for the first time in electrochemical capacitors. Based on the proposed 3D model, the resistance of the electrolyte, the membrane resistance, and the resistance of the current collectors and active materials can increase the first intersection points on the real axis (*x*-axis) of the Nyquist plots. Also, the results revealed a novel phenomenon where the initial and final points of the CV curves shift up and the shape of CV curves is pushed inward a little by changing the leakage resistance and the resistance of the faradaic part of the materials. These results can explain which parameters play a major role in deformation of the CV shape from the ideal state. The experimental results confirmed that the proposed model is completely correct, in that the change of any of the aforementioned parameters indeed increased the first intersection point on the *x*-axis of the

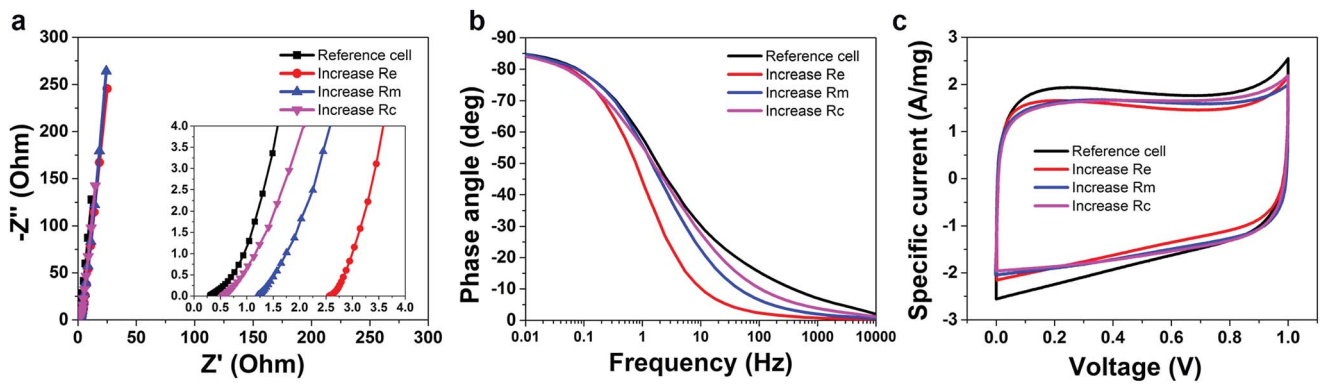

Fig. 9 (a) EIS plot, (b) the phase angle *versus* frequency and (c) CV curves at a scan rate of 20 mV s^{-1} of the real material.

Nyquist plot and also affected the shape of the CV curves. To improve the performance of ECs based on the reported results, the selected electrolyte should have the highest ionic conductivity, the chosen membrane should have a sufficient size of porosity based on the electrolyte to get the lowest ionic resistivity, the current collector should have the highest conductivity with good surface interactions with the active material and the active material should have the highest electrical conductivity. The leakage resistance depends on the packaging of the cell, so packaging methods play an important role in the final result. Finally, the faradaic part of the active material can improve the capacity of the EC by helping the choice of the best candidate with high capacitance and low resistive behaviour (if R_{CT} is high in the material, it provides capacity with low resistive behaviour).

Conflicts of interest

There are no conflicts to declare.

Acknowledgements

This research was co-sponsored by the National Research Foundation of South Africa (Grant Number: 61056). All findings, conclusions or recommendations expressed in this work are solely those of the author(s). The NRF does not accept liability in any regard.

References

1 H. Ibrahim, A. Ilinca and J. Perron, *Renewable Sustainable Energy Rev.*, 2008, **12**, 1221–1250.
2 C. Shen, Y. Xie, B. Zhu, M. Sanghadasa, Y. Tang and L. Lin, *Sci. Rep.*, 2017, **7**, 14324.
3 P. Simon and Y. Gogotsi, *Nat. Mater.*, 2008, **7**, 845–854.
4 J. Pu, F. Cui, S. Chu, T. Wang, E. Sheng and Z. Wang, *ACS Sustainable Chem. Eng.*, 2014, **2**, 809–815.
5 H. Jiang, P. S. Lee and C. Li, *Energy Environ. Sci.*, 2013, **6**, 41–53.
6 F. Barzegar, A. Bello, J. K. J. K. Dangbegnon, N. Manyala and X. Xia, *Appl. Energy*, 2017, **207**, 417–426.
7 F. Barzegar, J. K. J. K. Dangbegnon, A. Bello, D. Y. D. Y. Momodu, A. T. C. T. C. Johnson and N. Manyala, *AIP Adv.*, 2015, **5**, 097171.
8 Y. Wang, Y. Song and Y. Xia, *Chem. Soc. Rev.*, 2016, **45**, 5925–5950.
9 F. Wang, X. Wu, X. Yuan, Z. Liu, Y. Zhang, L. Fu, Y. Zhu, Q. Zhou, Y. Wu and W. Huang, *Chem. Soc. Rev.*, 2017, **46**, 6816–6854.
10 T. Purkait, G. Singh, D. Kumar, M. Singh and R. S. Dey, *Sci. Rep.*, 2018, **8**, 640.
11 D. W. Lee, J. H. Lee, N. K. Min and J.-H. Jin, *Sci. Rep.*, 2017, **7**, 12005.
12 B.-A. Mei and L. Pilon, *Electrochim. Acta*, 2017, **255**, 168–178.
13 A. B. Cultura and Z. M. Salameh, Modeling, Evaluation and Simulation of a Supercapacitor Module for Energy Storage Application, *International Conference on Computer Information Systems and Industrial Applications (CISIA)*, 2015, pp. 876–882.
14 O. Bohlen, J. Kowal and D. U. Sauer, *J. Power Sources*, 2007, **173**, 626–632.
15 L. Zubieta and R. Bonert, *IEEE Trans. Ind. Appl.*, 2000, **36**, 199–205.
16 N. Ber, J. Sabatier, O. Briat and J.-M. Vinassa, *IEEE Trans. Ind. Electron.*, 2010, **57**, 3991–4000.
17 W. Lajnef, J.-M. Vinassa, O. Briat, S. Azzopardi and E. Woirgard, *J. Power Sources*, 2007, **168**, 553–560.
18 A. Hammar, P. Venet, R. Lallemand, G. Coquery and G. Rojat, *IEEE Trans. Ind. Electron.*, 2010, **57**, 3972–3979.
19 S.-M. Park and J.-S. Yoo, *Anal. Chem.*, 2003, **75**, 455A–461A.
20 M. E. Orazem and B. Tribollet, *Electrochemical Impedance Spectroscopy*, John Wiley & Sons, 2011.
21 H.-K. Song, H.-Y. Hwang, K.-H. Lee and L. H. Dao, *Electrochim. Acta*, 2000, **45**, 2241–2257.
22 H. He, R. Xiong and J. Fan, *Energies*, 2011, **4**, 582–598.
23 A. Rahmoun, H. Biechl and A. Rosin, *Electr. Contr. Commun. Eng.*, 2013, **2**, 34–39.
24 Z. J. Han, D. H. Seo, S. Yick, J. H. Chen and K. Ostrikov, *NPG Asia Mater.*, 2014, **6**, e140.
25 F. Barzegar, A. Bello, O. O. Fashedemi, J. K. Dangbegnon, D. Y. Momodu, F. Taghizadeh and N. Manyala, *Electrochim. Acta*, 2015, **180**, 442–450.
26 S. Buller, E. Karden, D. Kok and R. W. De Doncker, in *Thirty-sixth IAS annual meeting*, IEEE, 2001, vol. 4, pp. 2500–2504.
27 K. Sheng, Y. Sun, C. Li, W. Yuan and G. Shi, *Sci. Rep.*, 2012, **2**, 247.